High-pressure behavior of FeOCl

Maxim Bykov,[1] Elena Bykova,[2,3] Sander van Smaalen,[1,*] Leonid Dubrovinsky,[3] Catherine McCammon,[3]
Vitali Prakapenka,[4] and Hanns-Peter Liermann[5]

[1]*Laboratory of Crystallography, University of Bayreuth, 95440 Bayreuth, Germany*
[2]*Material Physics and Technology at Extreme Conditions, Laboratory of Crystallography, University of Bayreuth, 95440 Bayreuth, Germany*
[3]*Bayerisches Geoinstitut, Universität Bayreuth, 95440 Bayreuth, Germany*
[4]*Center for Advanced Radiation Sources, University of Chicago, Chicago, Illinois 60637, USA*
[5]*Photon Sciences, FS-PE, Deutsches Elektronen Synchrotron (DESY), 22607 Hamburg, Germany*

(Received 28 November 2012; revised manuscript received 14 June 2013; published 22 July 2013)

A pressure-induced phase transition of FeOCl is discovered to occur at $P_c = 15 \pm 1$ GPa. It is preceded by extremely anisotropic lattice compression, which is explained by a gradual collapse of the van der Waals gap between the chlorine atoms on the borders of the slabs of this layered compound. Single-crystal x-ray diffraction in a diamond anvil cell is used to show that the high-pressure phase can be described as a fourfold superstructure with monoclinic lattice distortion, described by a $4a \times 1b \times 2c$ supercell with space group $B2_1/m$ (b unique). The high-pressure crystal structures have been used to uncover the mechanism of the phase transition, as the formation of alternating regions of increased packing density of chlorine atoms within a single layer and regions of interpenetrating layers. Raman and Mössbauer spectroscopies indicate that the phase transition is not related to electronic effects or magnetic order.

DOI: 10.1103/PhysRevB.88.014110 PACS number(s): 61.50.Ks, 61.05.cp, 64.30.−t

I. INTRODUCTION

The class of isostructural layered compounds MOX (M = Ti, V, Cr, Fe; X = Cl, Br) has been recently studied for their low-dimensional magnetic properties. It was shown that the behavior strongly depends on the number of d electrons of the transition-metal atom. While FeOCl, VOCl and CrOCl exhibit antiferromagnetic ordering with different types of superstructures at low temperatures,[1–7] TiOCl undergoes two phase transitions forming a spin-Peierls state below 67 K.[8–10]

High-pressure studies on TiOCl and TiOBr have lead to the discovery of two high-pressure phase transitions.[11–19] The transition at $P_{c1} \approx 13$–15 GPa is characterized by a sudden decrease of the semiconducting band gap and the formation of a twofold superstructure.[11,14,15,18] A second pressure-induced phase transition was predicted by theory and it has been observed through the occurrence of additional superlattice reflections in x-ray powder diffraction at pressures above $P_{c2} \approx 22$ GPa.[15,17] The origin of these phase transformations is still under discussion, but it is clear that the natures of low-temperature and high-pressure phase transitions are different.

FeOCl is a low-dimensional Mott insulator at ambient conditions.[20] The compound undergoes a paramagnetic-to-antiferromagnetic phase transition at $T_N = 81$ K.[1–4] The transition is accompanied by a monoclinic distortion of the orthorhombic lattice and the formation of an incommensurate magnetic superstructure.[1]

Another interest of FeOCl is related to its intercalation properties. Among layered compounds with a van der Waals gap metal oxyhalides have been widely used as host lattices.[21–27] Intercalation enables confining guest molecules or polymer chains in a well-defined environment. The resulting intercalation hybrids often exhibit novel magnetic and electronic properties. From this point of view, application of high pressure can provide a controlled method for varying material properties. Recently it was shown that the charge transfer in polyaniline-intercalated FeOCl can be enhanced through the application of external pressure.[27] A pressure-induced increase in conductivity in the FeOCl intercalated compounds could be of interest for their application as cathode materials. Although such intercalated systems are intensively studied, there is no information on the behavior of pure FeOCl under high pressure.

Here we report the discovery of a pressure-induced phase transition of FeOCl at $P_c = 15 \pm 1$ GPa, which is preceded by extremely anisotropic lattice compression. X-ray diffraction is used to show that the high-pressure phase is a fourfold superstructure of the structure below P_c, while its lattice symmetry is reduced from orthorhombic to monoclinic. The mechanism of the phase transition is related to an antiphase buckling of consecutive layers, resulting in regions of increased packing density of chlorine atoms of single layers and regions with interpenetrating chlorine layers, similar to soft layered materials.[28] The lowering of the symmetry at the phase transition is corroborated by Raman and Mössbauer spectroscopy. Furthermore, Mössbauer spectroscopy excludes magnetic order, while Raman spectroscopy indicates that the insulating behavior is retained at high pressures.

II. EXPERIMENT

Single crystals of FeOCl were prepared by gas transport from a stoichiometric mixture of $FeCl_3$ (purity 99.99%) and Fe_2O_3 (purity 99.999%).[1,29] Samples for the Mössbauer experiment (∼66.6% enriched in ^{57}Fe) were synthesized using a mixture of $FeCl_3$ and $^{57}Fe_2O_3$.

Pressure-dependent angle-dispersive powder x-ray diffraction measurements were carried out at beamline 13ID-D of the Advanced Photon Source (Chicago, USA) using monochromatic radiation of wavelength 0.3344 Å. The sample was put into a diamond anvil cell (DAC) with 250 μm diamond culets. A Re gasket with initial thickness 29 μm and 125 μm hole diameter was used. Ne served as a pressure-transmitting

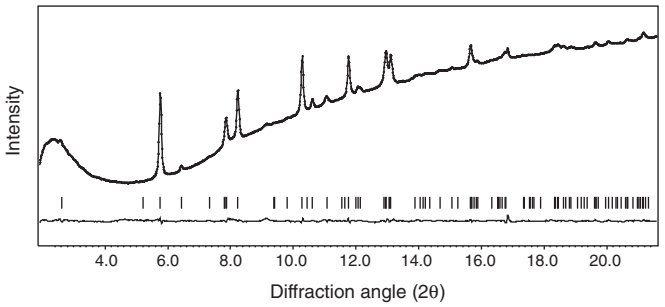

FIG. 1. Powder x-ray diffraction diagram at 4.9 GPa together with the Le Bail fit and the difference between measured and calculated intensities (lower trace). Vertical bars show the calculated peak positions.

medium. Pressure was determined by the change of the lattice parameters of Au using the equation of state reported by Fei *et al.*[30] Diffraction patterns were collected with a Mar165 CCD detector and integrated with FIT2D.[31] Le-Bail fits were performed with the JANA2006[32] for the determination of the lattice parameters as a function of pressure.

A single-crystal x-ray diffraction experiment was performed at beamline P02.2 of PETRA III (Hamburg, Germany), employing a wavelength of 0.29004 Å and pressures of 15.0 and 22.7 GPa. A BX90 DAC[33] with a large opening angle of $4\theta = 80^\circ$ was used together with 250 μm Boehler-Almax diamonds, a Re gasket with 29 μm initial thickness and 130 μm hole, and Ne as a pressure-transmitting medium.[34] Diffracted intensity was collected on a Mar345 image plate detector and then processed with the CrysAlisPro software package,[35] resulting in integrated intensities for 106 main reflections and 200 first-order satellite reflections (15 GPa data set), and 101 main reflections, 201 first-order and 102 second-order satellite reflections (22.7 GPa data set).

Raman scattering experiments were performed with a LabRam spectrometer (resolution 2 cm^{-1}), equipped with a 15 mW HeNe laser (wavelength 632.8 nm) and a 50× objective. The pressure was measured by ruby fluorescence.[36] Raman spectra were measured with the sample in a DAC at 13 selected pressures in the range 3–38 GPa.

^{57}Fe Mössbauer spectra were recorded at room temperature in transmission mode on a constant acceleration Mössbauer spectrometer with a nominal 370 MBq ^{57}Co source in a 12-μm-thick Rh matrix. The velocity scale was calibrated relative to a 25-μm-thick α-Fe foil. Spectra were measured at five selected pressures between 0 and 19.5 GPa. Each spectrum took 4 to 7 days to collect. Peaks were described by Lorentzian line shapes using the software package MOSSA.[37]

III. RESULTS

A. Powder x-ray diffraction

The powder x-ray diffraction patterns could be indexed according to the orthorhombic FeOCl lattice with space group *Pmmn* (Fig. 1). However, a significant broadening of the diffraction maxima was observed in patterns collected at pressures above 15 GPa. Furthermore, the pressure dependencies of the lattice parameters exhibit small anomalies at the same pressure, resulting in apparently different compressibilities

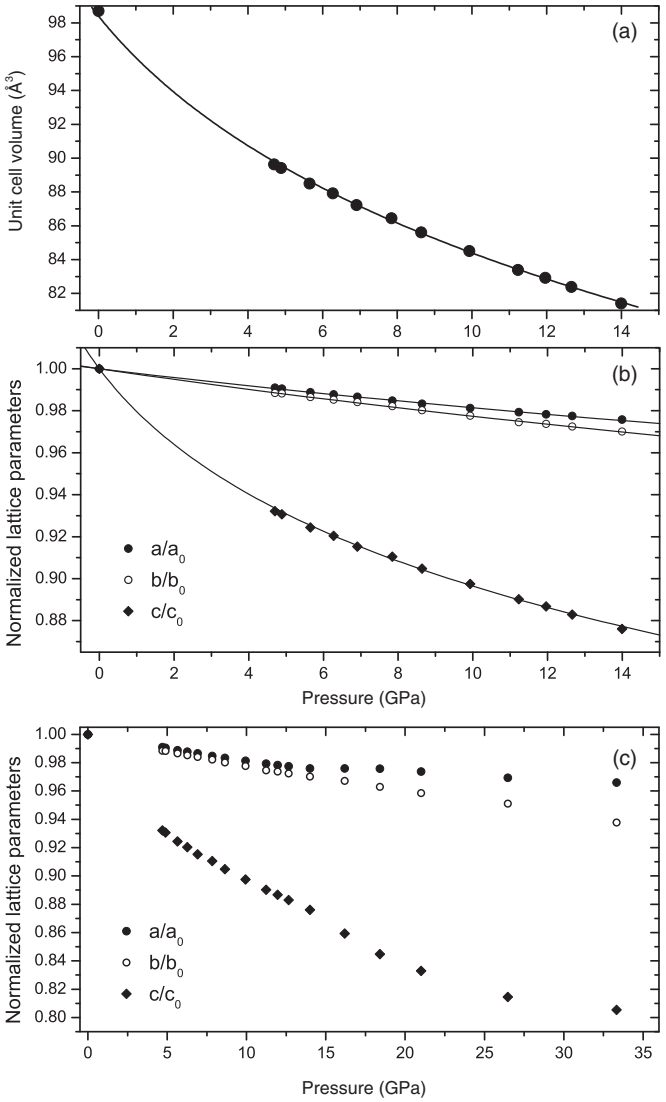

FIG. 2. (a) Pressure dependence of the unit cell volume. (b) Pressure dependence of normalized lattice parameters in the range 0–15 GPa. Solid curves represent the fits of Eq. (1) to the experimental data. (c) Pressure dependence of the normalized lattice parameters over the whole pressure range studied.

above and below 15 GPa [Fig. 2(c)]. Most notable is the very small pressure dependence of a at high pressures, with a nearly constant value within the range 15–18 GPa.

These effects suggest the occurrence of a phase transition at ∼15 GPa, as it is confirmed by Raman and Mössbauer spectroscopies and single-crystal x-ray diffraction (see below). However, the weak anomalies do not constitute proof of a phase transition by themselves, because nonhydrostatic conditions above 15 GPa for neon as pressure-transmitting medium[38] might also contribute to apparent anomalies in pressure-dependent experiments. In addition, the present powder x-ray diffraction experiments failed to detect the structural changes as observed by single-crystal x-ray diffraction (Sec. III C), mainly due to extremely preferred orientation of the sample, with the platelike crystallites lying flat on top of the diamonds, resulting in the **c** axis being parallel to the x-ray beam.

TABLE I. Linear and volume bulk moduli of FeOCl.

	K_0 (GPa)	K'
Volume	36(3)	8.2(8)
a axis	153(4)	5.3(9)
b axis	127(6)	4.0[a]
c axis	13.0(5)	4.9(2)

[a]Fixed.

The volume-pressure dependence up to 14 GPa was described with a third-order Birch-Murnaghan equation of state [Fig. 2(a)]:[39]

$$P = 3K_0 f_E(1+2f_E)^{5/2}[1+3/2(K'-4)f_E], \quad (1)$$

where $f_E = [(V/V_0)^{2/3}-1]/2$. The fit to the data resulted in the bulk modulus $K_0 = 36\,(3)$ GPa, zero-pressure volume $V_0 = 98.3\,(4)$ Å^3, and $K' = 8.2\,(8)$.[40]

For the description of linear compressibilities the parametric form of the Birch-Murnaghan equation of state was used, substituting the cube of the lattice parameter for the volume.[41] Both the graphical representation [Fig. 2(b)] and the bulk moduli (Table I) indicate an extremely anisotropic compressibility.

B. Raman spectroscopy

The full representation of the vibrational modes of FeOCl in space group $Pmmn$ is

$$\Gamma_{\text{tot}} = 3A_g + 2B_{1u} + 3B_{2g} + 2B_{2u} + 3B_{3g} + 2B_{3u}. \quad (2)$$

The modes with symmetries A_g, B_{2g}, and B_{3g} are Raman active. Two strong modes have been observed in the Raman spectra taken at low pressures [Fig. 3(b)]. They can be identified with A_g modes according to Ref. 42. Their Raman shifts gradually increase with pressure up to 15 GPa [Fig. 3(a)]. Two additional modes are present in Raman spectra at pressures above 15 GPa [Figs. 3(a) and 3(c)]. This confirms a phase transition at ∼15 GPa, and it suggests a lowering of crystal symmetry at the transition, in agreement with the results of single-crystal x-ray diffraction.

The observation of resonance peaks in the Raman spectra indicates that FeOCl is nonmetallic at all pressures. Visual inspection of the sample within the DAC showed FeOCl to remain transparent, a further indication for the insulating character at all pressures.

C. Single-crystal x-ray diffraction

Superlattice reflections were observed in the diffraction at both pressures, 15.0 and 22.7 GPa. Most conveniently, the superstructure can described by a nonconventional B-centered, eightfold $4a \times b \times 2c$ pseudo-orthorhombic supercell. Due to unavoidable incompleteness of the data arising from limitations imposed by the DAC, the superspace approach[43,44] can be used to increase the ratio between the number of unique reflections and the number of refined parameters. Within this approach the high-pressure structure of FeOCl can be described by the orthorhombic superspace group $Pmmn(\sigma_1,0,\frac{1}{2})00s$ [No. 59.1.10.6 with standard setting

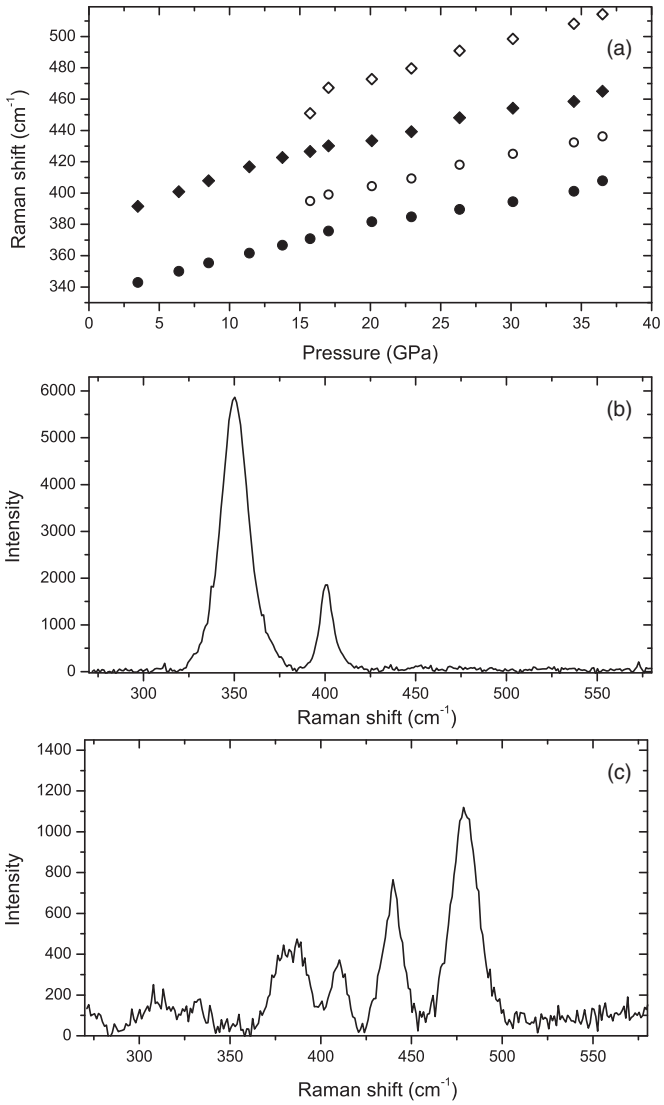

FIG. 3. (a) Pressure dependence of Raman peak shifts of FeOCl. At pressures above 15 GPa, additional peaks were observed (open symbols). (b) Raman spectra at 6.4 GPa and (c) at 23.0 GPa.

$Pmnm(0,\frac{1}{2},\sigma_3)000$][45,46] and commensurate modulation wave vector $\mathbf{q} = (\frac{1}{4},0,\frac{1}{2})$.

The crystal structure is described by the coordinates of the three unique atoms, μ = Fe, O, Cl, with respect to the orthorhombic basic-structure unit cell, with $a(15) = 3.675(8)$, $b(15) = 3.191(2)$, and $c(15) = 6.803(10)$ Å at 15 GPa, and $a(22.7) = 3.631(2)$, $b(22.7) = 3.170(1)$, and $c(22.7) = 6.551(15)$ Å at 22.7 GPa. Positions of the atoms in the superstructure are then obtained as the sum of the basic-structure position $\bar{\mathbf{x}}(\mu)$ and values of the modulation functions $\mathbf{u}^{\mu}(\bar{x}_4)$:

$$\mathbf{x}(\mu) = \bar{\mathbf{x}}(\mu) + \mathbf{u}^{\mu}(\bar{x}_4), \quad (3)$$

where $\bar{x}_4 = t + \mathbf{q}\cdot\bar{\mathbf{x}}(\mu)$, and the parameter t represents the phase of the modulation. Displacive modulations of atom μ are described by truncated Fourier series:

$$u_i^{\mu}(\bar{x}_4) = \sum_{n=1}^{n_{\max}} A_i^n(\mu)\sin(2\pi n\bar{x}_4) + B_i^n(\mu)\cos(2\pi n\bar{x}_4), \quad (4)$$

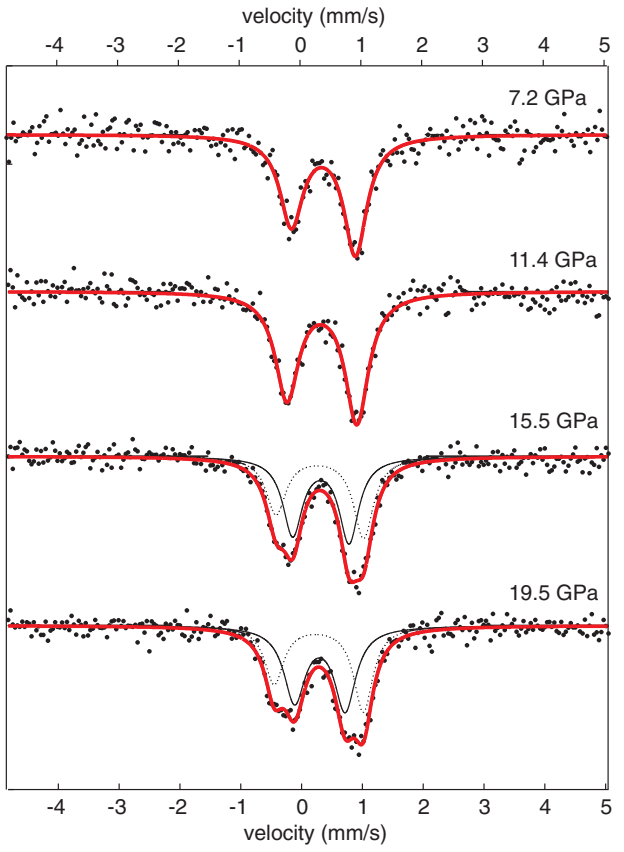

FIG. 4. (Color online) High-pressure Mössbauer spectra of ^{57}Fe measured on FeOCl powder samples in a DAC.

for $i = x,y,z$, with $n_{\max} = 1$ for 15.0 GPa, and $n_{\max} = 3$ for 22.7 GPa.

The atomic coordinates of the ambient-pressure $Pmmn$ structure model of FeOCl[47] were used as a starting point for the refinements of the basic structures against main reflections at both pressures. Subsequently, modulation parameters $A_i^n(\mu)$ and $B_i^n(\mu)$ were given arbitrary but small starting values. Refinement of all parameters against all reflections exhibited a smooth convergence, eventually leading to good fits to the diffraction data with $R_{\text{all}} = 0.0578$, $R_{\text{main}} = 0.0443$, and $R_{\text{sat1}} = 0.1053$ at 15.0 GPa, and $R_{\text{all}} = 0.0529$, $R_{\text{main}} = 0.0400$, $R_{\text{sat1}} = 0.0693$, and $R_{\text{sat2}} = 0.0541$ at 22.7 GPa (sat1 and sat2 refer to first- and second-order satellite reflections, respectively).

Different sections t of superspace lead to different symmetries of the $4a \times b \times 2c$ supercell. They are Bm, $B2_1/m$ (both are **b** unique), and $Bmm2$. The best fit to the diffraction data was achieved for $t = 1/16$, which corresponds to the centrosymmetric, monoclinic space group $B2_1/m$ (No. 11 with standard setting $P2_1/m$).[48]

The possible symmetries are the same as those implied by the irreducible representation A3 of space group $Pmmn$ at $\mathbf{k} = (\frac{1}{4},0,\frac{1}{2})$, which defines the symmetry of the primary distortion for this phase transition.[49] The necessity of high-order harmonics ($n_{\max} = 3$) within the superspace approach means that in addition to the primary order parameter, secondary order parameters contribute to the structural distortion at higher pressures without further symmetry breaking.

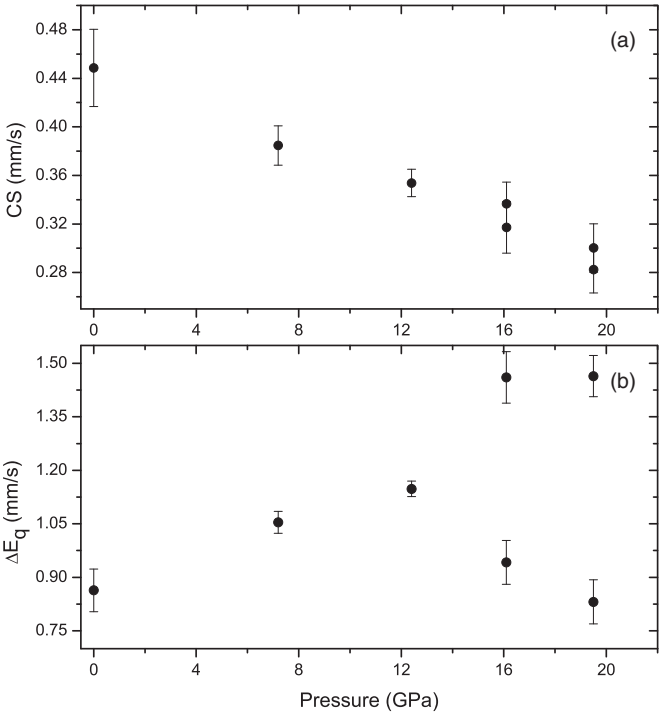

FIG. 5. Pressure dependence of (a) the CS and (b) the quadrupole splitting in Mössbauer spectra.

D. Mössbauer spectroscopy

The Mössbauer spectra below 15 GPa exhibit a single doublet, which can perfectly be fitted by a pair of Lorentzian functions (Fig. 4). The center shift (CS) of the Fe^{3+} doublet is consistent with its octahedral coordination and with previous studies at ambient conditions.[50] The observed decrease of the CS with pressure [Fig. 5(a)] is in agreement with the expected increase in s-electron density at the nucleus. Spectra at

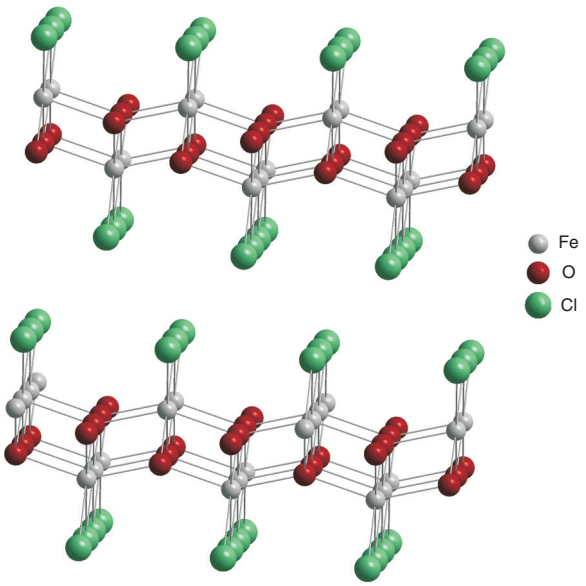

FIG. 6. (Color online) Basic structure of FeOCl. Layered crystal structure consisting of Fe-O double layers sandwiched by chlorine layers and separated by van der Waals gaps.

TABLE II. Atomic displacements (Å) from the basic structure positions along **a** and **c** axes at 15.0 and 22.7 GPa.

Atom	x-15GPa	x-22.7 GPa	z-15 GPa	z-22.7 GPa
Fe1	0.015	0.026	−0.11	−0.25
Fe2	−0.036	−0.074	−0.05	−0.13
Fe3	−0.015	−0.025	0.11	0.29
Fe4	0.036	0.073	0.05	0.09
O1	0.034	0.036	−0.06	−0.14
O2	−0.014	−0.015	−0.14	−0.33
O3	−0.034	−0.036	0.06	0.14
O4	0.014	0.015	0.14	0.33
Cl1	0.035	0.115	−0.17	−0.25
Cl2	−0.153	−0.407	−0.03	−0.12
Cl3	−0.132	−0.237	0.12	0.33
Cl4	0.250	0.529	0.09	0.04

pressures above 15 GPa did not show any evidence of magnetic ordering. However, they cannot be described by a single doublet. Instead, they show two, partially overlapping doublets with nearly equal CSs and different quadrupole splittings, indicating the presence of more than one independent Fe site, in agreement with the model for the superstructure.

IV. DISCUSSION

A. Anisotropic compressibility

The large anisotropy of the compressibility is related to the layered crystal structure of FeOCl. The structure can be described in terms of Fe-O double layers sandwiched between Cl layers thus forming slabs that are stacked along the crystallographic **c** axis.[47] The slabs are formed by sharing O-O and O-Cl edges of the distorted *cis*-FeO_4Cl_2 octahedra and they are connected by weak van der Waals interactions (Fig. 6). The latter directly explain that the compressibility along the **c** axis is several times larger than that along the **a** and **b** axes (Fig. 2).

A quantitative analysis of the crystal structures shows that the interlayer Cl-Cl distance at ambient pressure, 3.680 Å, is close to twice the van der Waals radius of chlorine. The linear compressibility along **c** is in a good agreement with the compressibility of molecular Cl_2 [$K_0 = 14.2(24)$ GPa] reported by Dusing *et al.*,[51] and with the linear compressibilities of layered $FeCl_2$ [$K_0 = 16(3)$ GPa] and TiOCl [$K_0 = 12(1)$ GPa].[15,52] These similarities show that the linear bulk moduli of FeOCl (Table I), $FeCl_2$, and TiOCl and the volume bulk modulus of Cl_2 directly represent the compressional behavior of Cl-Cl van der Waals bonds. Differences between these values arise from differences in the packing of Cl atoms within the layer, from different partial charges on Cl atoms, and from the rigidity of layer backbone itself.

The compressibility along **a** reflects the reduction of Fe-O distances. Since chemical bonds are the least compressible feature of crystal structures, this explains that **a** is the most incompressible direction in FeOCl (Table I). On the other hand, the compressibility along **b** is related to the contraction of the Fe_2OCl quadrangles, which is achieved through a pressure dependence of Fe-O-Fe and Fe-Cl-Fe bond angles. Bond angles are generally more soft than bond lengths are.

B. High-pressure crystal structures

The high-pressure phase of FeOCl contains four crystallographic sites for each atom (denoted as Fe1-Fe4, Cl1-Cl4 and O1-O4), while the atomic connectivity and coordination numbers remain the same as those of the crystal structure at ambient conditions. Mössbauer spectra distinguishes only two Fe sites of different quadrupole splittings (Fig. 4). This discrepancy is explained by the details of the superstructures as defined by the atomic shifts out of the basic *Pmmn* structure. Iron and oxygen atoms pairwise have shifts of nearly equal magnitude and opposite direction (Table II), thus suggesting pairwise similar quadrupole fields at the Fe sites. The four chlorine atoms all have different shifts that reflect the greater flexibility of these atoms within the van der Waals gaps.

The superstructures of FeOCl at pressures of 15.0 and 22.7 GPa are compared to the structure at ambient conditions in Fig. 7. The superstructures reveal an antiphase buckling of the Fe-O bilayers, with a noticeable variation of the interlayer distances that increases with pressure. Fe and O atoms do not possess large displacements along **a** due to the rigidity of the Fe-O bonds (Sec. IV A). However, the buckling of the layers

TABLE III. Selected interatomic distances (Å) and angles (deg). Given are the average values (Ave), the minimum and maximum values for the high pressure phase at 15.0 and 22.7 GPa, as well as distances and angles for the ambient pressure phase (AP).

	15 GPa			22.7 GPa			
	Min	Max	Ave	Min	Max	Ave	AP
Fe-Fe	3.007(14)	3.031(13)	3.018(13)	2.960(20)	3.026(18)	2.993(19)	3.104(1)
Fe-Fe[a]	3.191(2)	3.191(2)	3.191(2)	3.170(1)	3.170(1)	3.170(1)	3.3046(7)
Fe-O[b]	1.85(2)	1.92(2)	1.89(2)	1.84(3)	1.92(3)	1.88(3)	1.964(8)
Fe-O[a]	2.059(14)	2.099(15)	2.079(13)	2.036(13)	2.116(13)	2.067(12)	2.100(10)
Fe-Cl	2.231(19)	2.31(2)	2.277(19)	2.27(2)	2.31(12)	2.28(2)	2.368(7)
Cl-Cl[c]	2.97(3)	3.06(3)	3.01(3)	2.91(3)	2.89(3)	2.92(3)	3.680(3)
O-Fe-O[b]	151.5(10)	152.1(10)	151.8(10)	150.1(9)	154.4(11)	152.8(10)	148.35(4)
Fe-O-Fe[b]	147.6(13)	155.9(13)	151.8(12)	143.5(11)	161.8(11)	152.8(11)	148.35(4)

[a]Along the **b** axis.
[b]Along the **a** axis.
[c]Interlayer distance.

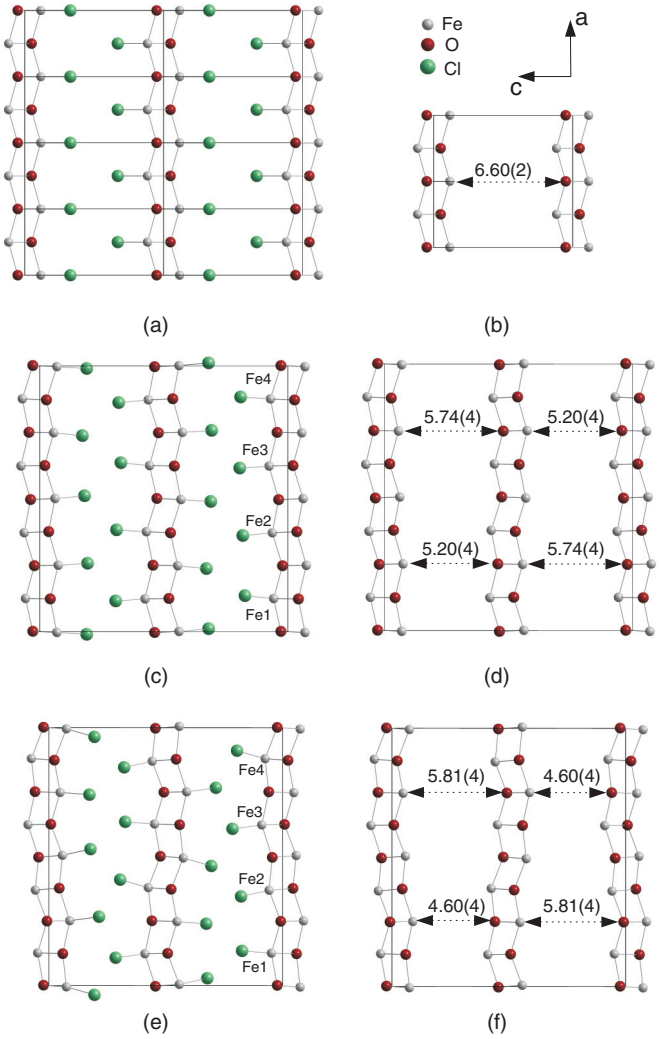

FIG. 7. (Color online) (a) Projection along **b** of the crystal structure of FeOCl at ambient conditions. (b) Distance (Å) between Fe-O double layers within the ambient phase. Chlorine atoms are not shown. (c) Projection along **b** of the high-pressure crystal structure at 15.0 GPa. (d) Minimum and maximum distances (Å) between Fe-O double layers in the high-pressure phase at 15 GPa. Chlorine atoms are not shown. (d) Projection along **b** of high-pressure crystal structure at 22.7 GPa. (e) Minimum and maximum distances (Å) between Fe-O double layers in the high-pressure phase at 22.7 GPa. Chlorine atoms are not shown.

is clearly represented by in-phase displacements of Fe and O atoms along **c** (Table II). It can be related to a variation of the Fe-O-Fe bond angles (Table III). The compression of FeOCl is mainly determined by a decrease of the Cl-Cl distances (Table III). Within the high-pressure phase this affects both interlayer and intralayer distances, as it is governed by the large displacements of the chlorine atoms (Table II).

Higher pressures lead to a noticeable increase of the amplitudes of atomic displacements, and the regions of layer separation and interpenetration become more pronounced (Fig. 7). One can expect a saturation of the modulation amplitudes at higher pressures. However, we could not continue single-crystal diffraction studies at higher pressures, because the crystal was destroyed in our experiment by pressures higher than 22.7 GPa.

C. Mechanism of the phase transition

We propose that the driving force of the phase transition is related to the Cl-Cl interactions. At ambient conditions the interlayer Cl-Cl distances are close to the sum of their van der Waals radii, while the intralayer Cl-Cl distances are larger, because they are defined by rigid Fe-O framework. So, FeOCl is to a certain extent a frustrated system, since an optimal packing of Cl atoms is not be realized. Up to P_c, the packing density of chlorine is increased by a large decrease of interlayer Cl-Cl distances. The Fe-O framework is much more rigid, so that the intralayer Cl-Cl van der Waals contacts are hardly affected by pressure. The distortions defining the superstructure of the high-pressure phase allow an increase of both the interlayer and intralayer packing density in two ways. First, regions exist of increased of intralayer Cl-Cl distances. This allows for interpenetration of layers and each Cl atom of one layer is exclusively coordinated to Cl atoms of the neighboring layer. Within the other regions, the intralayer Cl-Cl distances are decreased, such that their distances are optimized. The antiphase buckling of the layers within the high-pressure phase leads to both types of regions, as it is apparent from Figs. 7(c)–7(f). Thus, initially soft van der Waals Cl-Cl distances are optimized in such a way that their variation at high pressures is comparable to the variations of the lengths of the rigid Fe-O bonds (Table III). This situation is similar to that observed at low temperatures for soft layered materials $(C_3H_7NH_3)_2MCl_4$ with M = Cu, Mn.[28]

The proposed mechanism for the high-pressure phase transition of FeOCl is essentially different from the mechanism proposed for TiOCl, where the phase transition is attributed to spin-Peierls-like interactions between Ti^{3+}, followed by the formation of superstructures, involving doubling of **b** and alternation of Ti-Ti distances.[18] The symmetry of the single filled d orbital of Ti^{3+} allows exchange interactions along the Ti chains parallel to **b** only, and thus is responsible for the formation of the spin-Peierls state.[8,53] On the other hand, Fe^{3+} has five unpaired d electrons. The additional electrons enter d orbitals of different symmetries that are responsible for strong interchain exchange interactions on the ab plane.[50,54] Accordingly, antiferromagnetic order is energetically preferred over the formation of spin-singlet pairs. The observed $4a \times 1b \times 2c$ supercell of FeOCl does not allow for a variation of Fe-Fe distances along the ribbons parallel to **b** (Table III), and it thus is in agreement with the absence of spin-singlet pairs within the HP phase.

The structural phase transition of FeOCl does not bear obvious relations to a supposed insulator-metal transition. Raman spectroscopy has indicated the insulating character of FeOCl at all pressures. However, the continuous reduction of Fe-Fe distances and the changes of Fe-O-Fe bond angles certainly may affect the band structure and may lead to a reduction of a band gap. They do not exclude the possibility of metallization at even higher pressure than considered in the present work.

On the other hand, the proposed model of partial interpenetration of chlorine layers may also contribute to the

pressure-induced phase transitions in TiOCl. This alternative interpretation of the mechanism of the transition in TiOCl may explain the discrepancies between experimental data on high-pressure behavior of TiOCl from different sources. In this regard, high-pressure single-crystal x-ray diffraction of TiOCl would be highly desirable.

V. CONCLUSIONS

We have discovered a pressure-induced phase transition of FeOCl at $P_c = 15 \pm 1$ GPa. The phase transition is preceded by an extremely anisotropic lattice compression, which is explained by the gradual collapse of the van der Waals gap between the chlorine atoms at the borders of the slabs of this layered compound.

Crystal structures obtained by high-pressure single-crystal x-ray diffraction have been used to derive a microscopic mechanism of the phase transition. It is proposed that the high-pressure phase attains a denser packing of the chlorine atoms through a buckling of the layers. Consecutive layers with antiphase buckling lead to regions of increased packing density of Cl atoms within single layers and other regions with increased distances between these Cl atoms, then allowing for interpenetration of the chlorine layers of neighboring slabs (Fig. 7).

Spectroscopic evidence has been obtained, which shows that the high-pressure phase transition of FeOCl is not related to the development of magnetic order or to metallisation of this material. The mechanism proposed here for the high-pressure phase transition of FeOCl might also play a role in the high-pressure phase transitions of TiOCl. Understanding the high-pressure behavior of TiOCl would greatly benefit from high-pressure single-crystal x-ray diffraction experiments.

ACKNOWLEDGMENTS

Single crystals of FeOCl were grown at the Laboratory of Crystallography by Alfred Suttner. Financial support has been obtained from the German Science Foundation (DFG).

*smash@uni-bayreuth.de

[1] J. Zhang, A. Wölfel, L. Li, S. van Smaalen, H. L. Williamson, and R. K. Kremer, Phys. Rev. B **86**, 134428 (2012).
[2] R. W. Grant, J. Appl. Phys. **42**, 1619 (1971).
[3] E. Kostiner and J. Steger, J. Solid State Chem. **3**, 273 (1971).
[4] A. Adam and G. Buisson, Phys. Status Solidi A **30**, 323 (1975).
[5] A. Schönleber, J. Angelkort, S. van Smaalen, L. Palatinus, A. Senyshyn, and W. Morgenroth, Phys. Rev. B **80**, 064426 (2009).
[6] A. C. Komarek, T. Taetz, M. T. Fernández-Díaz, D. M. Trots, A. Möller, and M. Braden, Phys. Rev. B **79**, 104425 (2009).
[7] J. Angelkort, A. Wölfel, A. Schönleber, S. van Smaalen, and R. K. Kremer, Phys. Rev. B **80**, 144416 (2009).
[8] A. Seidel, C. A. Marianetti, F. C. Chou, G. Ceder, and P. A. Lee, Phys. Rev. B **67**, 020405(R) (2003).
[9] M. Shaz, S. van Smaalen, L. Palatinus, M. Hoinkis, M. Klemm, S. Horn, and R. Claessen, Phys. Rev. B **71**, 100405(R) (2005).
[10] A. Schönleber, S. van Smaalen, and L. Palatinus, Phys. Rev. B **73**, 214410 (2006).
[11] C. A. Kuntscher, S. Frank, A. Pashkin, M. Hoinkis, M. Klemm, M. Sing, S. Horn, and R. Claessen, Phys. Rev. B **74**, 184402 (2006).
[12] C. A. Kuntscher, S. Frank, A. Pashkin, H. Hoffmann, A. Schönleber, S. van Smaalen, M. Hanfland, S. Glawion, M. Klemm, M. Sing, S. Horn, and R. Claessen, Phys. Rev. B **76**, 241101 (2007).
[13] C. A. Kuntscher, M. Klemm, S. Horn, M. Sing, and R. Claessen, Eur. Phys. J. Special Topics **180**, 29 (2010).
[14] M. K. Forthaus, T. Taetz, A. Möller, and M. M. Abd-Elmeguid, Phys. Rev. B **77**, 165121 (2008).
[15] J. Ebad-Allah, A. Schönleber, S. van Smaalen, M. Hanfland, M. Klemm, S. Horn, S. Glawion, M. Sing, R. Claessen, and C. A. Kuntscher, Phys. Rev. B **82**, 134117 (2010).
[16] A. Prodi, J. S. Helton, Y. Feng, and Y. S. Lee, Phys. Rev. B **81**, 201103 (2010).
[17] Y.-Z. Zhang, H. O. Jeschke, and R. Valentí, Phys. Rev. Lett. **101**, 136406 (2008).
[18] S. Blanco-Canosa, F. Rivadulla, A. Piñeiro, V. Pardo, D. Baldomir, D. I. Khomskii, M. M. Abd-Elmeguid, M. A. López-Quintela, and J. Rivas, Phys. Rev. Lett. **102**, 056406 (2009).
[19] Y.-Z. Zhang, I. Opahle, H. O. Jeschke, and R. Valentí, J. Phys. Condens. Matter **22**, 164208 (2010).
[20] S.-H. Kim, J.-K. Kang, S. Hwang, and H. Kim, Bull. Korean Chem. Soc. **16**, 299 (1995).
[21] M. G. Kanatzidis, L. M. Tonge, T. J. Marks, H. O. Marcy, and C. R. Kannewurf, J. Am. Chem. Soc. **109**, 3797 (1987).
[22] M. G. Kanatzidis, C.-G. Wu, H. O. Marcy, D. C. DeGroot, C. R. Kannewurf, A. Kostikas, and V. Papaefthymiou, Adv. Mater. **2**, 364 (1990).
[23] J. F. Bringley, J.-M. Fabre, and B. A. Averill, J. Am. Chem. Soc. **112**, 4577 (1990).
[24] C.-G. Wu, D. C. DeGroot, H. O. Marcy, J. L. Schindler, C. R. Kannewurf, T. Bakas, V. Papaefthymiou, W. Hirpo, J. P. Yesinowski, Y.-J. Liu, and M. G. Kanatzidis, J. Am. Chem. Soc. **117**, 9229 (1995).
[25] I. Kargina and D. Richeson, Chem. Mater. **8**, 480 (1996).
[26] A. Sagua, E. Morán, M. A. Alario-Franco, A. Rivera, C. León, J. Santamaría, and J. Sanz, Int. J. Inorg. Mater. **3**, 293 (2001).
[27] I. Jarrige, Y. Q. Cai, S. R. Shieh, H. Ishii, N. Hiraoka, S. Karna, and W.-H. Li, Phys. Rev. B **82**, 165121 (2010).
[28] B. Doudin and V. Heine, J. Phys.: Condens. Matter **2**, 3237 (1990).
[29] H. Schäfer, F. E. Wittig, and M. Jori, Z. Anorg. Allg. Chem. **287**, 61 (1956).
[30] Y. Fei, A. Ricolleau, M. Frank, K. Mibe, G. Shen, and V. Prakapenka, Proc. Natl. Acad. Sci. USA **104**, 9182 (2007).
[31] A. Hammersley, *FIT2D—A 2-D Data Reduction and Analysis Program* (ESRF, Grenoble, France, 2004).
[32] V. Petricek, M. Dusek, and L. Palatinus, *Jana 2006. The Crystallographic Computing System* (Institute of Physics, Praha, Czech Republic, 2006).

[33]I. Kantor, V. Prakapenka, A. Kantor, P. Dera, A. Kurnosov, S. Sinogeikin, N. Dubrovinskaia, and L. Dubrovinsky, Rev. Sci. Instrum. **83**, 125102 (2012).

[34]A. Kurnosov, I. Kantor, T. Boffa-Ballaran, S. Lindhardt, L. S. Dubrovinsky, A. Kuznetsov, and B. H. Zehnder, Rev. Sci. Instrum. **79**, 045110 (2008).

[35]*Xcalibur/SuperNova CCD System, CrysAlisPro Software System, Version 1.171.36.28* (Agilent Technologies, Oxford, UK, 2012).

[36]H. K. Mao, J. Xu, and P. M. Bell, J. Geophys. Res. **91**, 4673 (1986).

[37]C. Prescher, C. McCammon, and L. S. Dubrovinsky, J. Appl. Crystallogr. **45**, 329 (2012).

[38]S. Klotz, J.-C. Chervin, P. Munsch, and G. Le Marchand, J. Phys. D Appl. Phys. **42**, 075413 (2009).

[39]F. Birch, Phys. Rev. **71**, 809 (1947).

[40]Ambient-pressure lattice parameters were taken from Ref. 1, where crystals of FeOCl were synthesized employing the same technique, equipment, and reagents as in the present study.

[41]R. J. Angel, Rev. Mineral. Geochem. **41**, 35 (2000).

[42]D. Fausti, T. T. A. Lummen, C. Angelescu, R. Macovez, J. Luzon, R. Broer, P. Rudolf, P. H. M. van Loosdrecht, N. Tristan, B. Büchner, S. van Smaalen, A. Möller, G. Meyer, and T. Taetz, Phys. Rev. B **75**, 245114 (2007).

[43]T. Janssen, A. Janner, A. Looijenga-Vos, and P. M. de Wolff, in *International Tables for Crystallography Vol. C*, edited by E. Prince (Kluwer Academic, Dordrecht, 2006).

[44]S. van Smaalen, *Incommensurate Crystallography* (Oxford University Press, Oxford, 2007).

[45]H. T. Stokes, B. J. Campbell, and S. van Smaalen, Acta Crystallogr. Sect. A **67**, 45 (2011).

[46]S. van Smaalen, B. J. Campbell, and H. T. Stokes, Acta Crystallogr. Sect. A **69**, 75 (2013).

[47]M. D. Lind, Acta Crystallogr. Sect. B **26**, 1058 (1970).

[48]T. Hahn, *International Tables for Crystallography Vol. A*, 5th ed. (Kluwer Academic, Dordrecht, 2002), pp.164–167.

[49]B. J. Campbell, H. T. Stokes, D. E. Tanner, and D. M. Hatch, J. Appl. Crystallogr. **39**, 607 (2006).

[50]Y. D. Dai, Z. Yu, Y. He, H. B. Huang, T. Shao, J. Lin, A. M. Ali, Z.-Y. Jiang, and Y.-F. Hsia, Chem. Phys. Lett. **358**, 473 (2002).

[51]E. F. Dusing, W. A. Grosshans, and W. B. Holzapfel, J. Phys. **45**, 203 (1984).

[52]G. K. Rozenberg, M. P. Pasternak, P. Gorodetsky, W. M. Xu, L. S. Dubrovinsky, T. Le Bihan, and R. D. Taylor, Phys. Rev. B **79**, 214105 (2009).

[53]T. Saha-Dasgupta, R. Valentí, H. Rosner, and C. Gros, Europhys. Lett. **67**, 63 (2004).

[54]S. Glawion, M. R. Scholz, Y.-Z. Zhang, R. Valentí, T. Saha-Dasgupta, M. Klemm, J. Hemberger, S. Horn, M. Sing, and R. Claessen, Phys. Rev. B **80**, 155119 (2009).